

ONE FILE COPY

(2)

GL-TR-90-0129

YAI-TR-101

Upper Atmosphere IR Radiation Modeling and Analysis

AD-A227 214

J. M. Sindoni
R. J. Healey
B. K. Yap

DTIC
ELECTE
SEP 25 1990
S D CS D

Yap Analytics, Inc.
594 Marrett Road
Lexington, MA 02173

14 May 1990

Scientific Report No. 1

APPROVED FOR PUBLIC RELEASE; DISTRIBUTION UNLIMITED

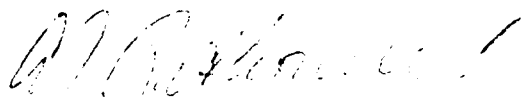
GEOPHYSICS LABORATORY
AIR FORCE SYSTEMS COMMAND
UNITED STATES AIR FORCE
HANSCOM AIR FORCE BASE, MASSACHUSETTS 01731-5000

90 09 24 014

"This technical report has been reviewed and is approved for publication"

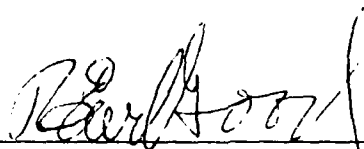


D. F. Kimball
Contract Manager
Atmospheric Backgrounds Branch
Optical and Infrared Technology Division



A. J. Ratkowski, Chief
Atmospheric Backgrounds Branch
Optical and Infrared Technology Division

FOR THE COMMANDER



R. EARL GOOD, SES, Director
Optical and Infrared Technology Division

This report has been reviewed by the ESD Public Affairs Office (PA) and is releasable to the National Technical Information Service (NTIS).

Qualified requestors may obtain additional copies from the Defense Technical Information Center. All others should apply to the National Technical Information Service.

If your address has changed, or if you wish to be removed from the mailing list, or if the addressee is no longer employed by your organization, please notify GL/IMA, Hanscom AFB, MA 01731. This will assist us in maintaining a current mailing list

Do not return copies of this report unless contractual obligations or notices on a specific document requires that it be returned.

FIGURE		PAGE
3	Theoretical fit of the squares of the absolute analytical and peaking t-matrices to the differential cross section ratio.....	11
4	Comparison of the exact and differential cross section with the analytical approach.....	12
5	Comparison of the vibrational temperature profiles of SHARC and RAD codes.....	20
6	Radiative pumping rate predicted by RAD code.....	21
7	Comparison of band radiances as predicted by SHARC and RAD.....	22
8	Comparison of SHARC prediction with SPIRE and SPIRIT data for NO.....	23
9	Comparison of SHARC prediction with SPIRE and SPIRIT data for O ₃	24
10	Comparison of SHARC prediction with SPIRE and SPIRIT data for CO ₂	25
A1	Plot of differential cross section.....	A12
A2	Plot of the ratio of the exact and PA differential cross sections.....	A13
A3	Total cross section.....	A14
B1	Direct and normalized reverse differential cross sections.....	B14
B2	Ratio of the forward and normalized reverse differential cross sections.....	B15
B3	Ratios of the forward and normalized reverse differential corss sections of N ₂	B16
B4	Threshold value for 1% deviation from sdb condition.....	B17
B5	Comparison of the differential cross sections for four models.....	B18

1. INTRODUCTION

This first annual report describes work completed by Yap Analytics, Inc. under contract F19628-89-C-0033 during the period from April 20, 1989 through April 30, 1990. Our objective is the study of the mechanisms involved in the emissions of the infrared (IR) radiation of the upper atmosphere and the related impacts of this background clutter on surveillance sensors. During this time frame, we concentrated our efforts on the investigation of the models for non-equilibrium phenomena leading to emission from very high rotational levels. One critical parameter in the model is the scattering cross section in a complex multi-body collision and interaction. In this investigation, the impulse approach (IA) is being applied to atom-molecule collisions which accounts for the total scattering amplitude of an atom incident upon a complex system by summation of independent two particle interactions. A resultant momentum distribution of each constituent particle is then evaluated. Studies to date by various investigators uses simplifications, the peaking approximation (PA), to evaluate the complex integral for the momentum of non-interaction (spectator) particles. Our work investigated the validity and accuracy of the PA.

During this period, we also worked on atmospheric code validation and compared code predictions with field measured data. In particular, we compared outputs of the SHARC code with the RAD code to understand the models used in each code, the discrepancies

of the models and the resultant differences in the code predictions. Adjustments of universal constants were made to the codes for comparison on an equal basis. A standard atmospheric profile was used as input to SHARC code to provide atmospheric radiance profile predictions for the NO, O₃, and CO₂ bands. Comparisons of these predictions were then made with field data measured on the SPIRIT and SPIRE programs.

2. ATMOSPHERIC MODELING AND ANALYSIS

The Impulse Approach (IA) to collisions was proposed as early as 1959. The theory suggests the total scattering for a projectile incident upon a complex system is the sum of the two-body amplitude between the projectile and each of the constituents of the complex system. Thus far we have confined our work to atom-diatom collisions. Previous computations have always been accomplished by using an additional approximation, called the peaking approximation (PA), to greatly simplify the formalism. We have, however, developed an exact impulse approach that does not rely on this approximation. The results obtained using our exact IA programs have been used for comparison with PA computations and with various experimental data. Additionally, the validity of IA has been determined by the properties of semi-detailed balancing and the optical theorem. These findings are detailed in the two papers included in Appendix A and B of this report, Impulse formalism for atom-molecule collisions: Inadequacy of the peaking approximation, published in the August 1, 1989 issue of Physical Review A, and Criteria for applicability of the impulse approach to collisions, which will appear in the next issue of the same publication.

2.1 Comparison of exact and PA results

Differential and total cross sections have been computed for various systems to evaluate the validity of the peaking approxi-

Taylor expanded t-matrix and the peaking t-matrix. Figure (3) superimposes the cross section ratios of Figure (1) with the ratio of the squares of absolute values of the analytical t-matrix and the peaking t-matrix. It is clear that the analytical expression for exact/PA provides an excellent approximation over nearly the entire range.

We have further examined the validity of this analytical treatment by comparing the exact and differential cross sections with those obtained using the analytical approach. Figure (4) displays the differential cross section based on the exact and analytical approach for the $\text{Li}^+ + \text{N}_2$ process $(0,0) \rightarrow (1,6)$ at 1 eV as a function of scattering angle. The two curves are nearly indistinguishable except for around 14° where the cross section almost vanishes.

In addition, we have tested the validity of the analytical approximation for many other systems, including $\text{H} + \text{N}_2$ and $\text{Li}^+ + \text{N}_2$ using various initial and final molecular states.

2.2 Assessing the validity of IA

Using the semi-detailed balance (sdb) condition, we have assessed the criteria for the applicability of the impulse approach. The sdb condition requires the cross sections in the forward direction and the normalized cross sections in the reverse directions to be equal. A violation of the sdb condition indicates an

internal inconsistency in IA, leading us to believe the approach is not valid. We have computed cross sections using our exact impulse approach for various systems in the forward and reverse directions, in particular $\text{Li}^+ + \text{N}_2 \leftrightarrow \text{Li}^+ + \text{N}_2 (v', j')$. Using the half-on-the-shell (post and prior) models of the two body t-matrix, we have shown that in both the IA leads to a violation of the sdb conditions for small scattering angles. The cross sections are studied quantitatively as a function of the relative translational energy and the mass of the incident particle. For large scattering angles we also find that the cross sections are independent of the choice of energy parameter ϵ_i (the kinetic energy of the colliding particles before the collision). We suggest that two criteria be used for assessing the validity of IA: 1) the sdb condition and 2) model independence, where each model is distinguished by the choice of ϵ_i in the two body t-matrix. The findings are detailed in our paper, Criteria for applicability of the impulse approach to collisions (Appendix B).

In addition to the sdb condition, we have also used the optical theorem to determine the validity of our current approach. This involves computing total cross sections (integrated over scattering angle) for all possible transitions from a given initial state and a fixed relative translational energy. This has been done for both the $\text{Li}^+ + \text{N}_2$ and $\text{H} + \text{N}_2$ systems using $(v=0, j=0)$ or $(v=0, j=12)$ as the initial state and 1 eV, 2 eV, and 4 eV as

the incident energies. The sum total of cross sections is then compared to the elastic scattering amplitude in the forward direction. Our findings suggest that the multiple collision terms may be necessary to satisfy the sdb and optical theorem conditions.

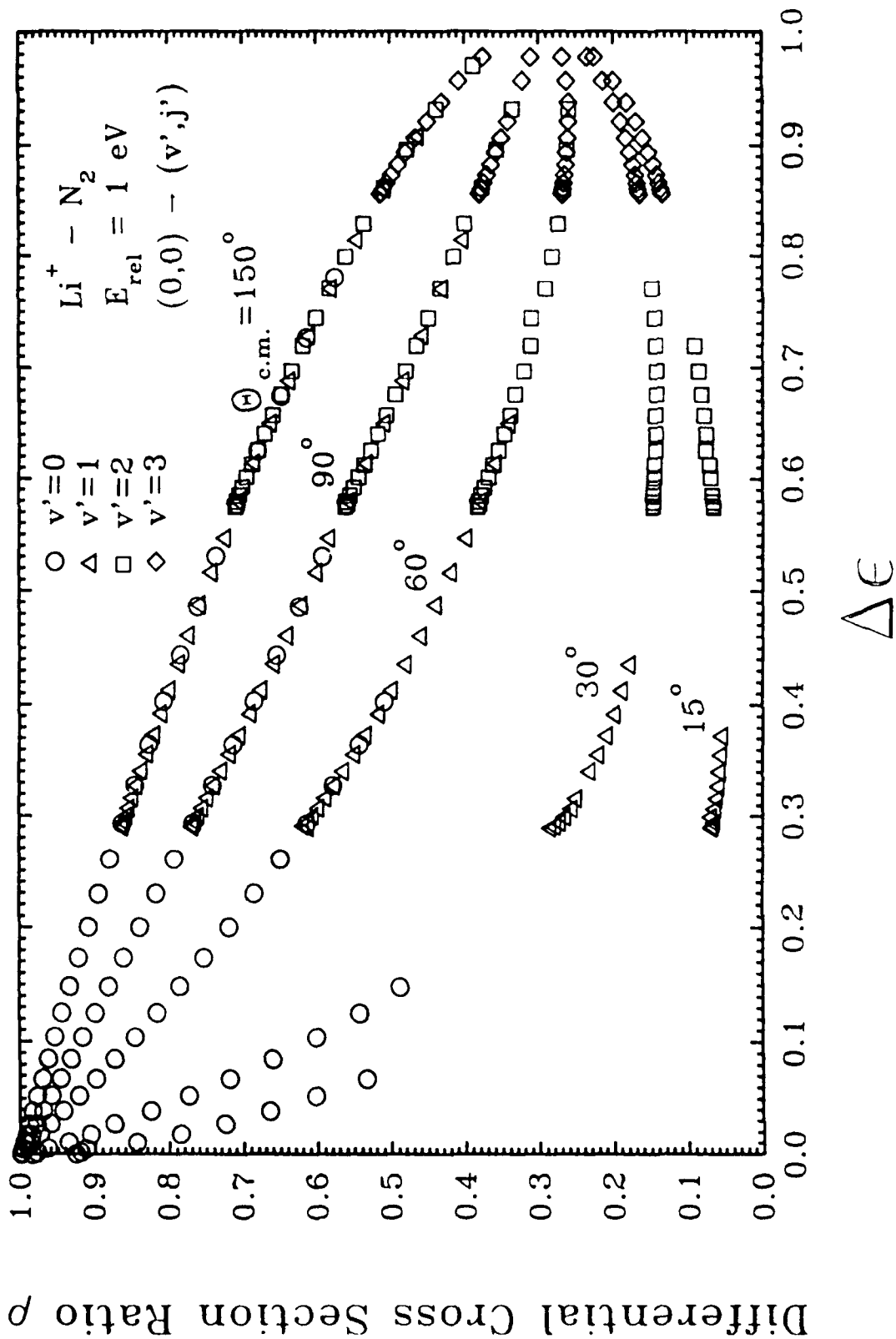


Figure 1. Differential cross section ratio for 1 eV and various scattering angles.

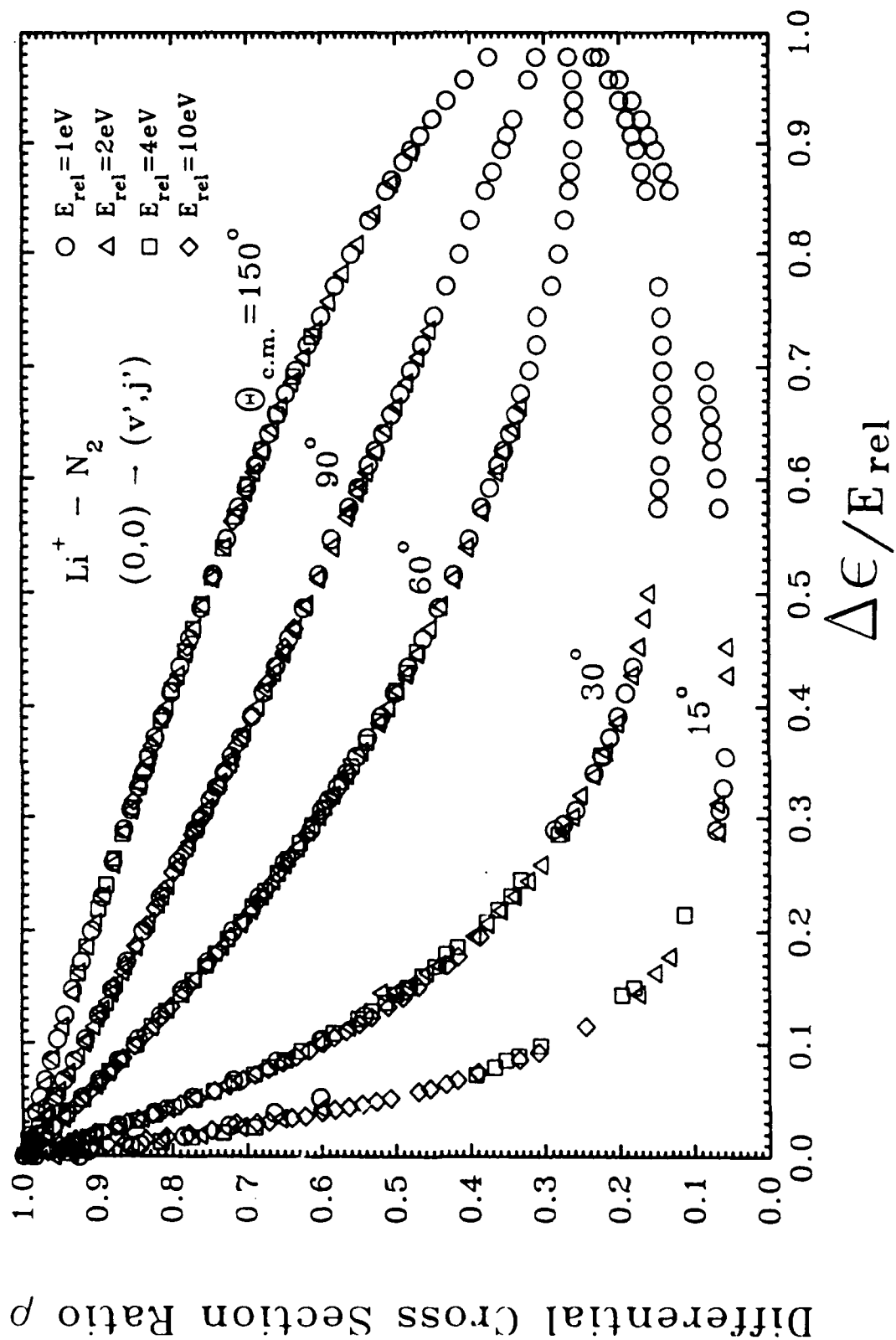


Figure 2. Differential cross section ratio at 1,2,4 and 10 eV and various scattering angles.

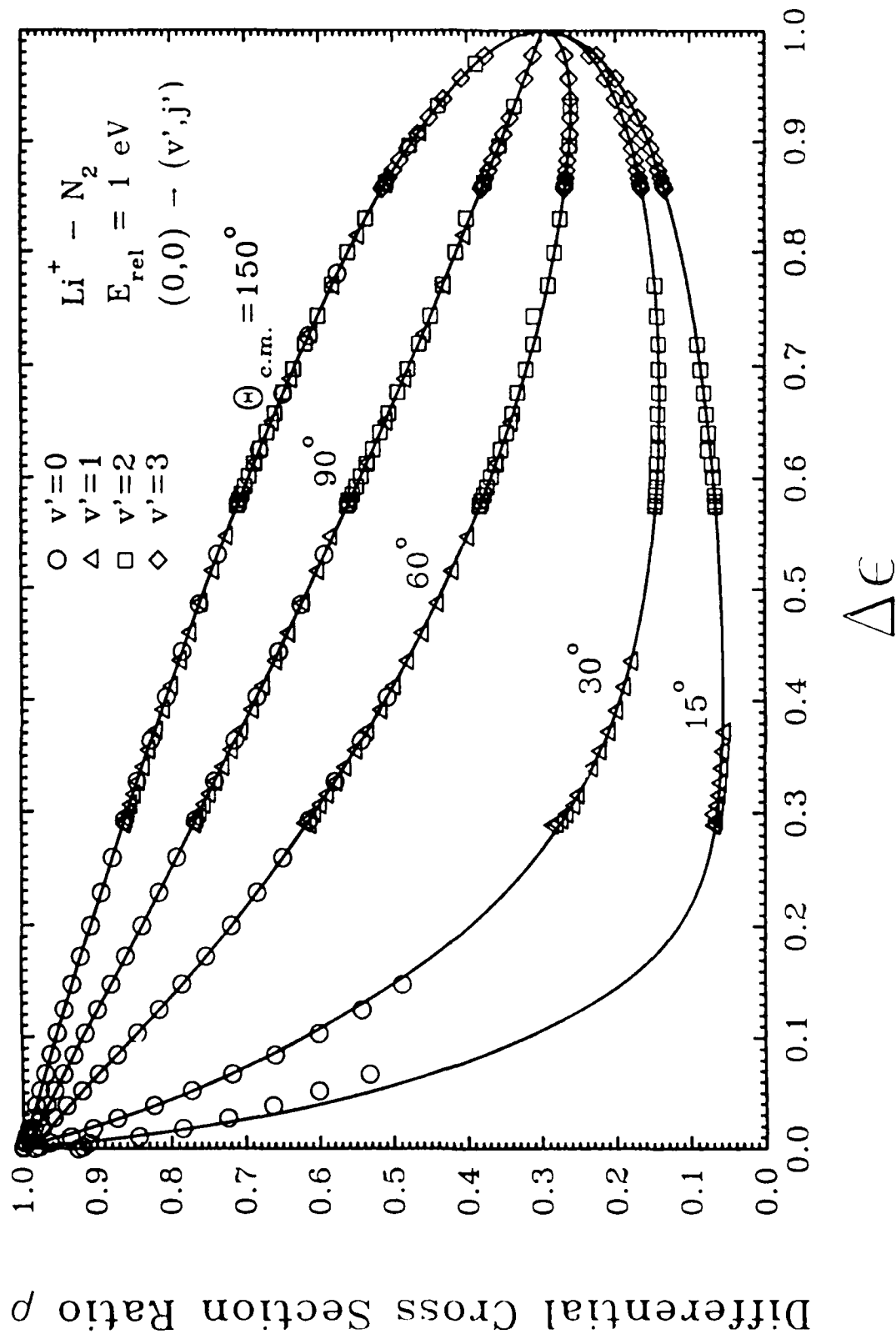


Figure 3. Theoretical fit of the squares of the absolute analytical and peaking t-matrices to the differential cross section ratio.

as the only emitter. The vibrational temperatures for the 626 isotope ν_2 (01101) level were compared with the output from the RAD program. At the lower altitudes, 60 km to 100 km, the differences between the two programs were relatively small and the values oscillated, sometimes SHARC had higher values but more often they were lower. At altitudes higher than 100 km, however, the differences became increasingly larger with the values obtained by SHARC being the lower of the two. At the highest altitude, 175 km, SHARC was 24.6 K lower than the vibrational temperature determined by the 6-1 code (RAD). The rate coefficients for the CO_2 transition 00001 \rightarrow 01101 were scrutinized. The expression found in SHARC for the N_2 and O_2 molecules rate constant was similar to the expressions found in RAD. However, the rate constant in SHARC for the O molecule was

$$1 \times 10^{-13} T^{1/2} + 2.32 \times 10^{-9} e^{-76.75/T^{1/3}} + 7.41 \times 10^{-14} e^{-1820/T} \quad (1)$$

while RAD used

$$1.5 \times 10^{-13} T^{1/2} + 2.32 \times 10^{-9} e^{-76.75/T^{1/3}} \quad (2)$$

Notice that for the dominant term of the expression SHARC had 1×10^{-13} whereas RAD had 1.5×10^{-13} as the coefficient. This coefficient in the expression for the rate constant in SHARC was changed to match that of RAD and SHARC was rerun. The same trend

was seen as in the first run but the temperatures were in closer agreement. Again the SHARC temperatures were lower and the most significant difference occurred at the highest altitude. At 175 km the temperature difference was 14.3 K.

Due to the continuing discrepancy between the codes the Einstein A coefficients were compared. New coefficients for SHARC were generated and the CO₂ linking file was changed to replace the coefficients with the new ones. The new Einstein A coefficients were compared with those found in the open literature and also with those in RAD. Most values compared favorably and only one Einstein A coefficient was found to effect this band emission and, therefore, it was examined more closely. The values were close enough and should not cause such a large discrepancy theoretically between the vibrational temperatures but SHARC was run again for the same case with the new Einstein A coefficients. These output values were very similar to the previous run. The largest discrepancy occurred again at the highest altitude where SHARC was 14.7 K lower than RAD.

In order to compare the excitation rates SHARC was run for an upwelling earthshine case. SHARC does not include in its output the collisional excitation rates but it does give the radiative excitation rates for the earth, sun, and atmosphere. RAD's output is given as a combination of these radiative excitation rates. Therefore, for a meaningful comparison the sum of the in-

dividual SHARC outputs was compared with RAD's output. Although discernable pattern emerged, many of SHARC's values were about half of those determined by the RAD code.

The three CO₂ input files used by SHARC were limited to only the information necessary for this one reaction. The Einstein A pertinent to this reaction was set to 1.525 for both codes. The reaction rate in SHARC for N₂/O₂ is

$$1 \times 10^{-16} T^{1/2} + 6.81 \times 10^{-8} e^{-82/T^{1/3}} \quad (3)$$

and Peter Wintersteiner of ARCON rearranged the expressions in the RAD code to match this. The first coefficient of 1.5E-13 was retained for the O for reaction rate. The problem still remained and the difference in temperature at 175 km was 11.0 K with SHARC being the lower of the two. Figure 5 shows these results.

One reason for the discrepancies in the vibrational temperatures is that SHARC uses a Doppler lineshape and RAD uses a Voigt lineshape. Emission that occurs at the lower altitudes can be absorbed at the higher altitudes. The Voigt lineshape has wings to account for this but the Doppler lineshape does not. Since the Doppler lineshape does not give the proper emission at the lower altitudes the absorption at the higher altitudes is too small. The Doppler shape, therefore, is giving lower temperatures than the Voigt shape.

The radiative pumping for each layer as seen from different

observation points in the atmosphere is given in RAD's output.

Looking at each observation point it can be determined which layers are producing the most pumping at each height. At the lower altitudes, the two layers closest to the altitude produce the most pumping but, at higher altitudes the largest contribution is from the total pumping below the lowest altitude (the blackbody contribution).

Figure 6 depicts the radiative pumping rate determined by RAD at 150 km tangent height as a function of altitude in fractional form. Each rate is divided by the total absorption at this height which is 1.93×10^4 photons/(sec-cm³). The total combined contribution from below 40 km as a fraction of the total is labelled as the blackbody contribution in Figure 6 and is the largest contributor to the total pumping at 150 km. The blackbody contribution is about 5.8 % of the total contribution. At high altitudes there is more absorption than at altitudes that fall in the middle (80-100 km) range. These middle range altitudes have a lower temperature which causes a narrow absorption cross-section and the blackbody contribution at these heights would be much less than at 150 km. The Voigt lineshape allows for this blackbody contribution, however, it is also important to note that while these radiative pumping values obtained from RAD give a very good indication of the importance of the wider wings it is still not an ideal model.

Vibrational Temperature Profiles

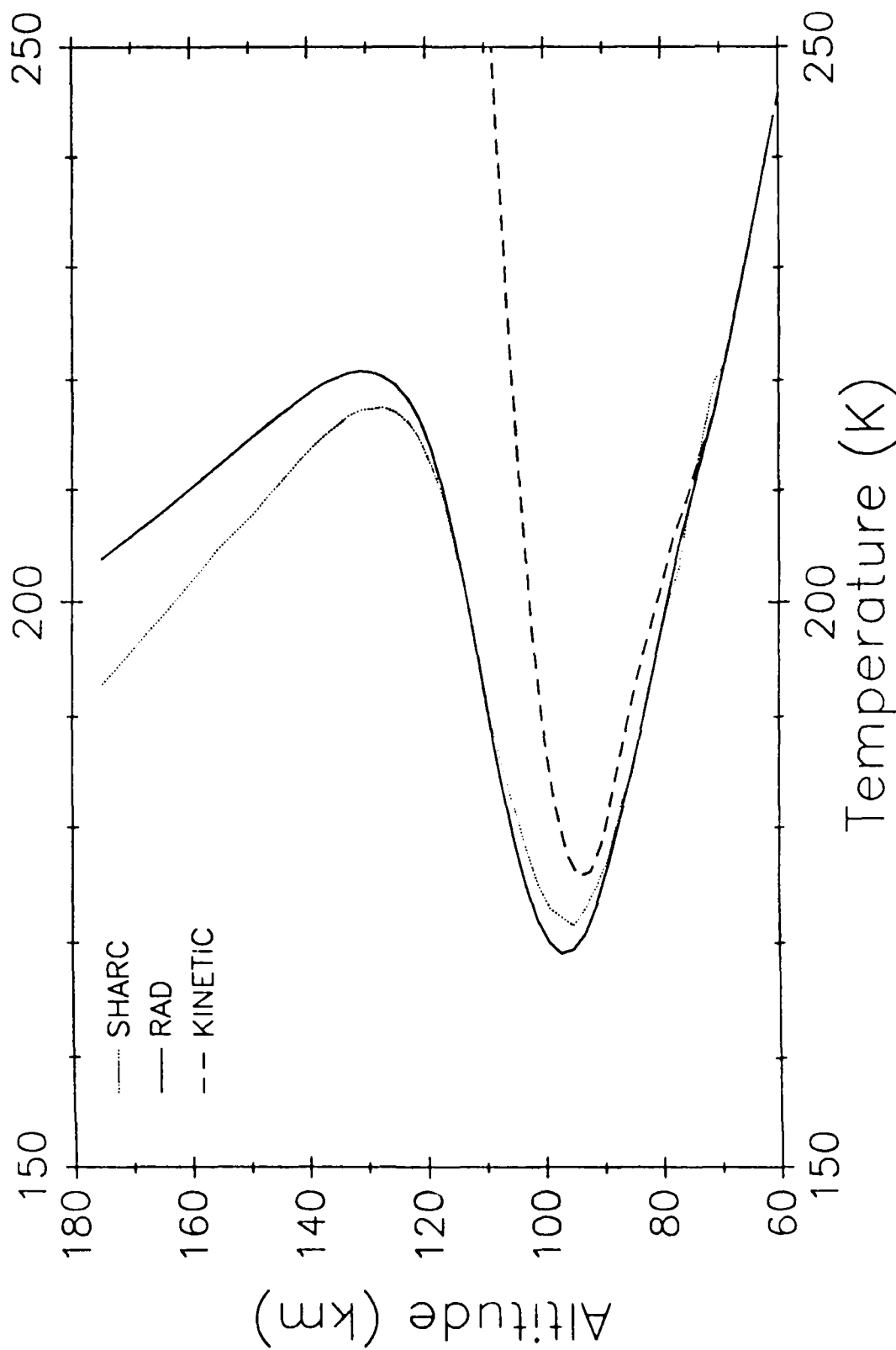


Figure 5. Comparison of the vibrational temperature profiles of SHARC and RAD codes.

Radiative Pumping Rate at 150 km as a function of altitude

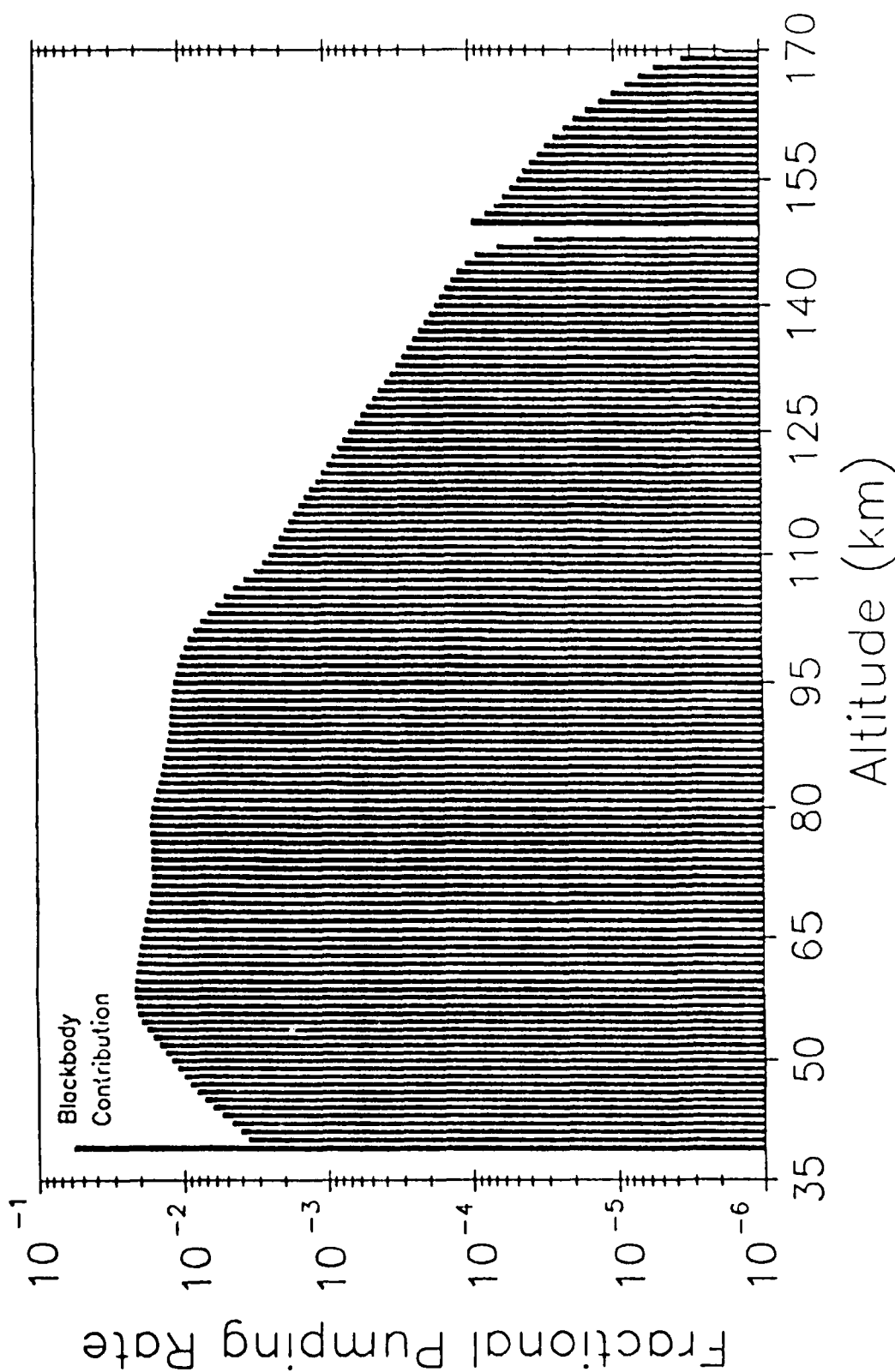


Figure 6. Radiative pumping rate predicted by RAD code.

Band Radiance Comparison at Various Tangent Heights

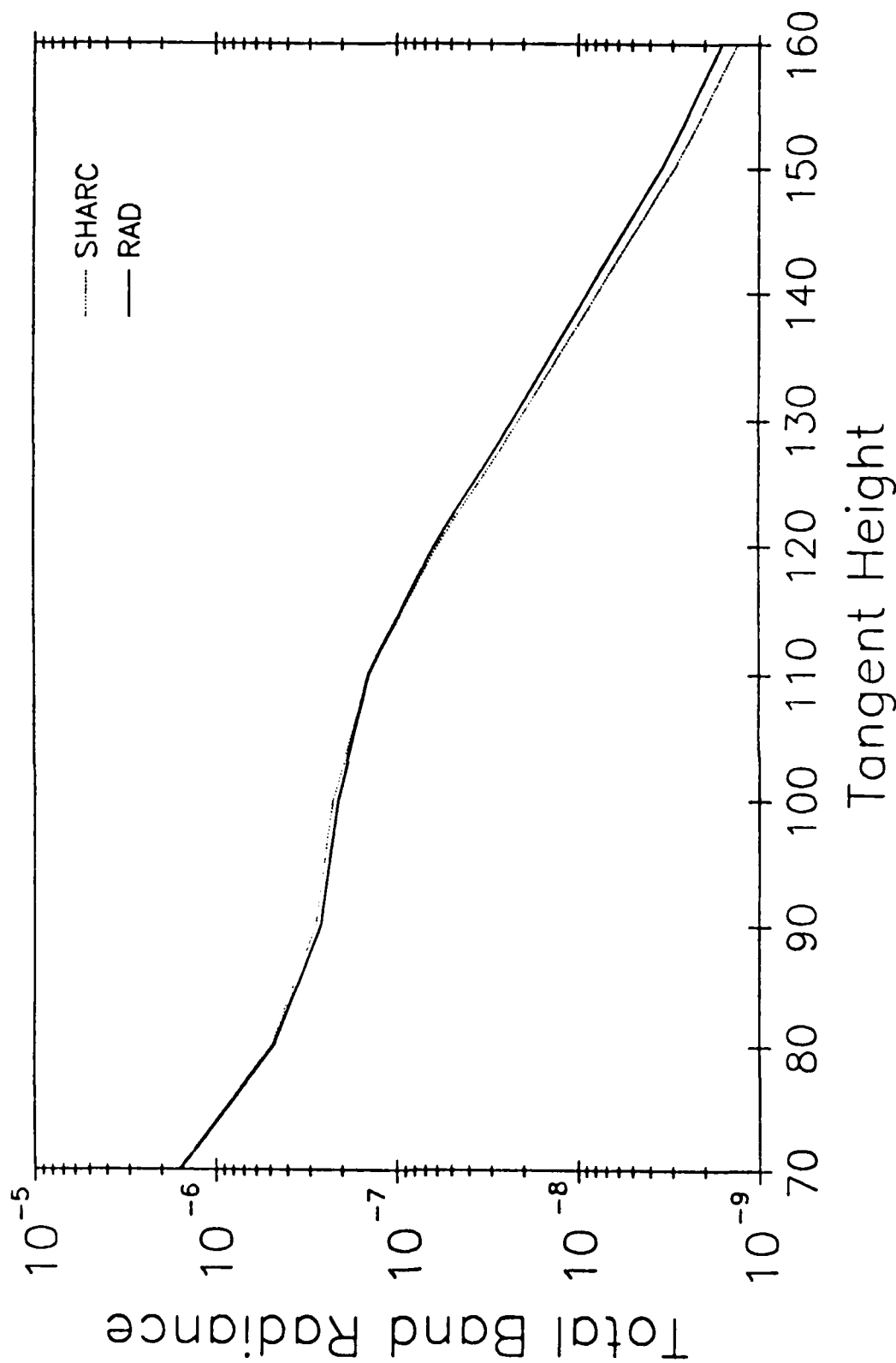


Figure 7. Comparison of band radiances as predicted by SHARC and RAD.

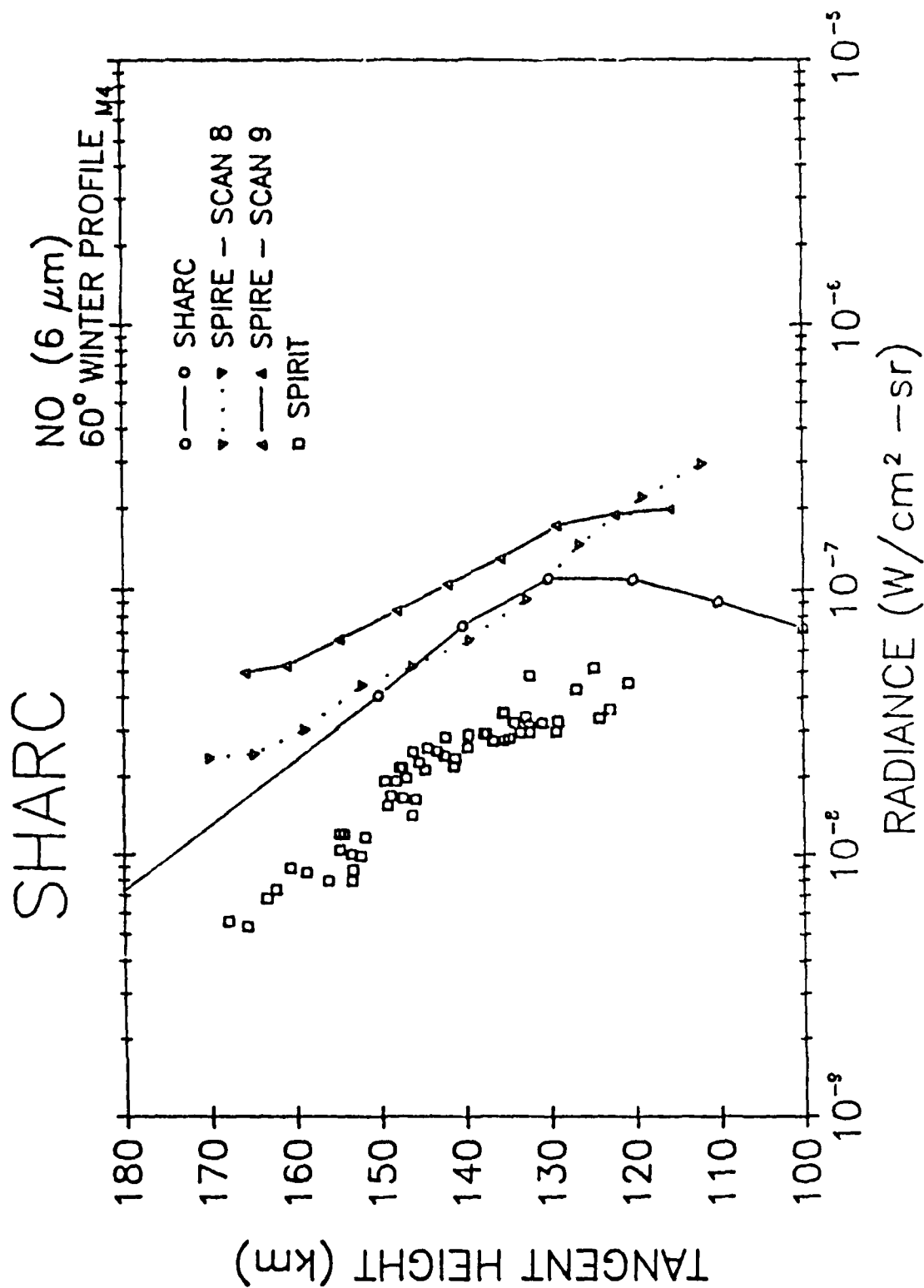


Figure 8. Comparison of SHARC prediction with SPIRE and SPIRIT data for NO.

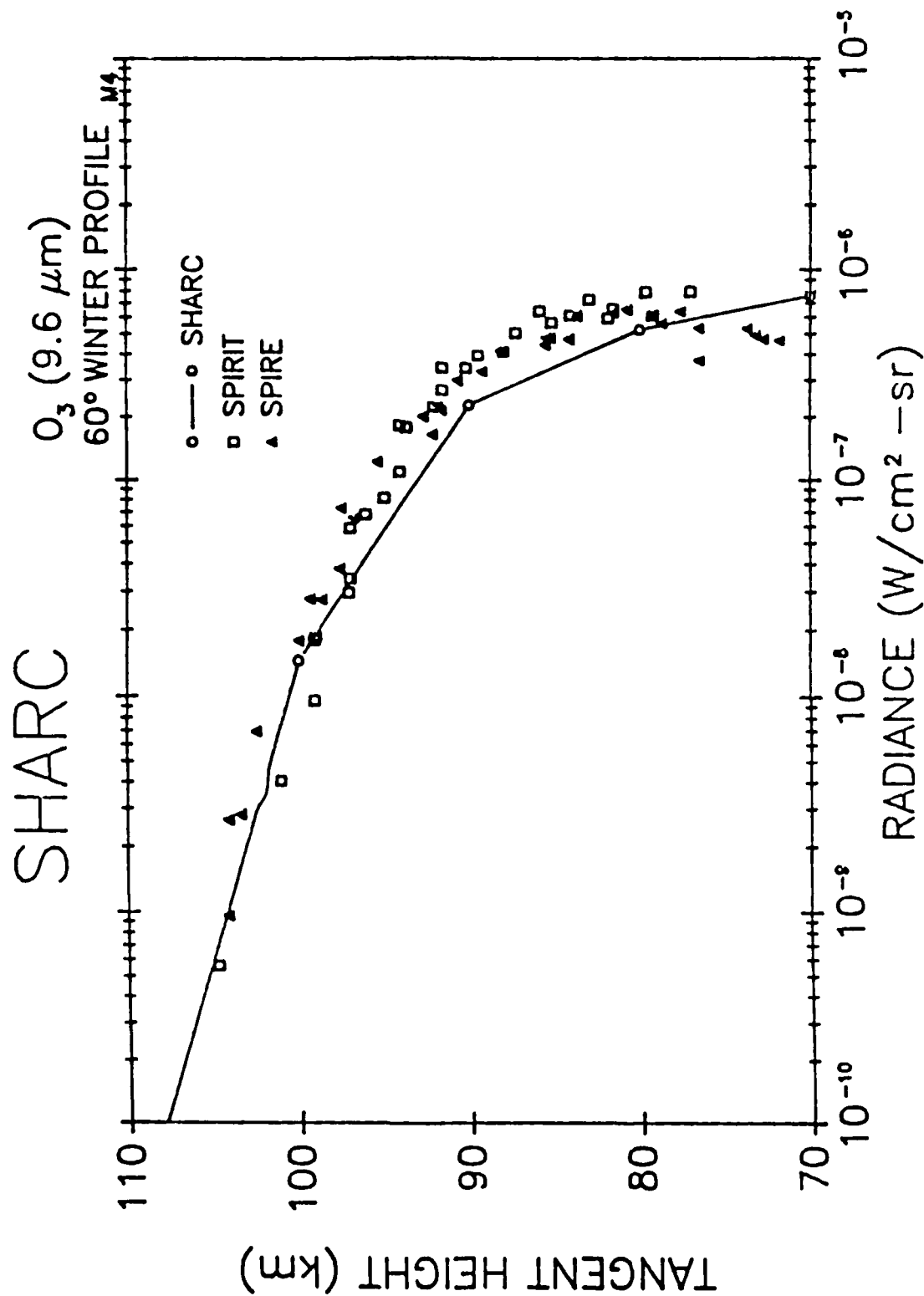


Figure 9 . Comparison of SHARC prediction with SPIRE and SPIRE data for O_3 .

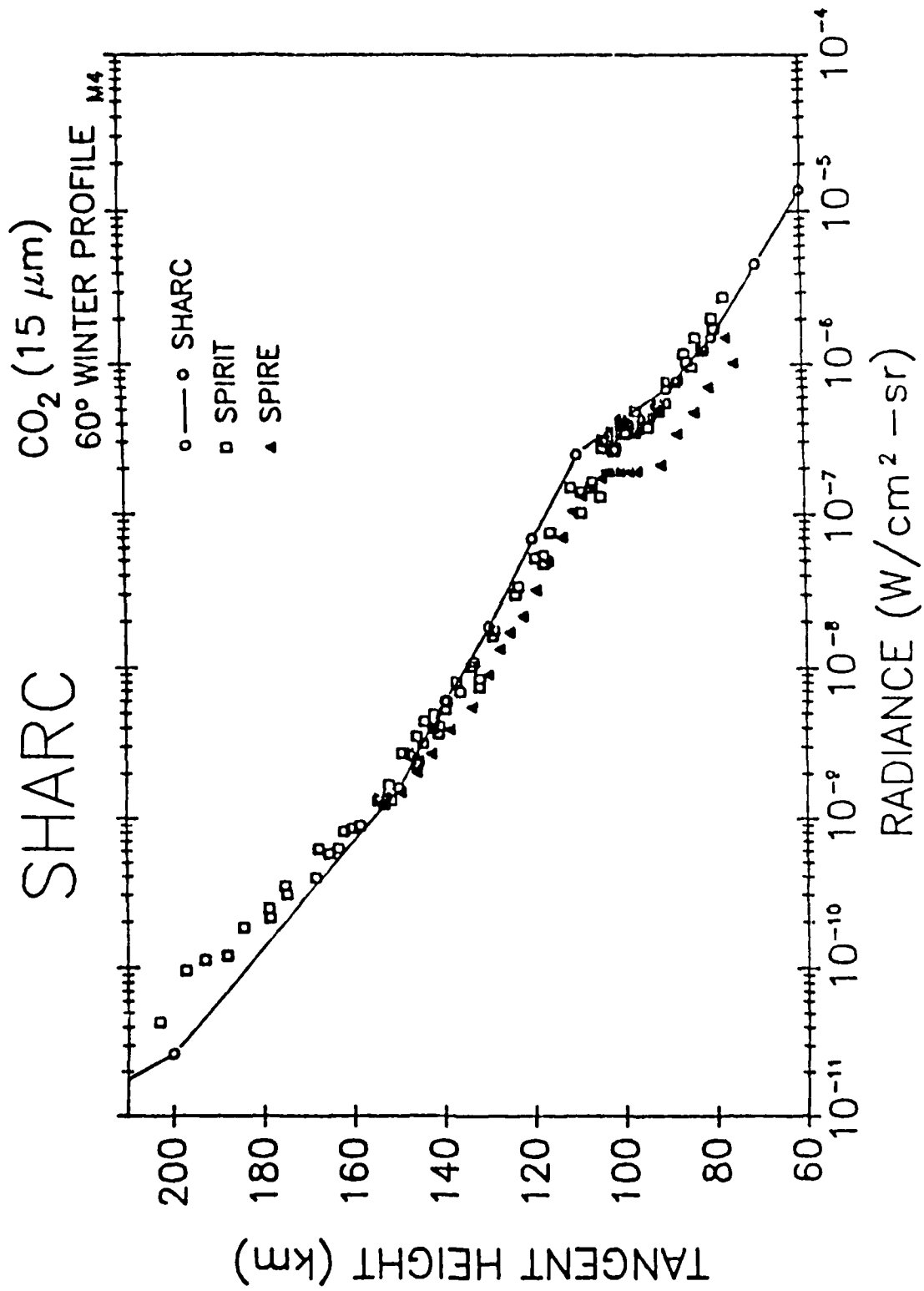


Figure 10. Comparison of SHARC prediction with SPIRE and SPIRE data for CO_2 .

APPENDIX A

Impulse Formalism For Atom-Molecule Collisions; Inadequacy of the Peaking Approximation.

Ramesh D.Sharma^a, Pradip M.Bakshi^b, and Joseph M.Sindoni^c.

a. Optical Physics Division, Geophysics Laboratory,

Hanscom Air Force Base, MA. 01890.

b. Physics Department, Boston College, Chestnut Hill, MA.02167.

c. Yap Analytics Inc., 594 Marret Road, Lexington, MA. 02173.

ABSTRACT

Expressions for differential and total cross-section for atom-diatom scattering are derived using the Impulse Formalism without any approximations. Results for the rotational-vibrational scattering are obtained, for the first time, without using the peaking approximation (PA). For the specific case of a hard core potential, it is shown that, except for elastic scattering, PA results are substantially different from the true impulse results.

The basic idea of Impulse Approach (IA) to collisions was proposed by Chew¹. The total scattering amplitude for a projectile incident upon a complex system is taken, in IA, to be the sum of the various two-body amplitudes-(the projectile plus each of the constituent particles of the complex system); the constituents not involved in the two-body scattering remain unaffected during the impact and are termed spectators. The role of the binding potential of the complex system is to generate a momentum distribution of the constituent particles. IA has been applied to atom-diatom collisions by Bogan², Eckelt, Korsch and Philipp³⁻⁶, and by Beard and Micha⁷.

In all of these papers an additional simplification, the Peaking Approximation (PA), is invoked to evaluate the integral over the spectator momentum. In this approximation, the t -matrix representing the two-body scattering process is evaluated for a particular value of the spectator momentum. This value of the spectator momentum is taken to be one for which the product of the initial and final state molecular wavefunctions is maximum. Since the two body t -matrix varies much more slowly with internal molecular momentum than does the product of the molecular wavefunctions, the integral over the spectator momentum factors into two parts : (i) two body t -matrix evaluated for a specific value of the spectator momentum, and, (ii) the molecular form factor integral which

can be evaluated easily for a given value of the momentum transferred. PA not only simplifies the computations but it also gives a very simple physical picture of the impulse formulation. However, its validity and accuracy have not been quantitatively assessed.

We have recently developed a formalism⁸ which permits computation of IA cross-sections without resorting to PA. This allows us to investigate the validity and assess the accuracy of PA. The purpose of this Rapid Communication is to point out that PA is valid only in the limited range of vibrationally and rotationally elastic scattering. It gives grossly erroneous overestimates for vibrationally inelastic forward scattering. It also does not converge to the true IA results even for high relative translational energies.

The state-to-state differential scattering cross-section for molecule 1-2 to undergo transition from initial vibration-rotation state v_j upon collision with atom 3 to final state $v'j'$ is given by^{3,5,8}

$$\frac{d\sigma}{d\Omega}(v_j p_3 \rightarrow v'j' p'_3, \theta) = \frac{p'_3}{p_3(2j+1)} \sum_m \sum_{m'} \left| \left(\frac{2\pi}{h} \right)^2 \mu_3 \langle \phi'_3 | \sum_{s=1,2} T^{(s)} | \phi_3 \rangle \right|^2 \quad (1)$$

where

$$\langle \phi'_3 | T^{(s)} | \phi_3 \rangle = \int d\vec{q}_3 \phi'_3(\vec{q}'_3) \langle \vec{q}'_s | t^{(s)} | \vec{q}_s \rangle \phi(\vec{q}_3) \quad (2)$$

and $|\phi_3\rangle \propto |v, j, m, \vec{p}_3\rangle$ is the initial state, the final state being denoted by primes. \vec{p}_3 and \vec{p}'_3 are the momenta of the incident particle before and after the collision in the center-of-mass (CM) frame of the atom-molecule system. \vec{p}_3 is also the momentum of the incident particle 3 with respect to the CM of the molecule 1-2. \vec{p}_a denotes the momentum of particle a with respect to the CM of bc and \vec{q}_a is the relative momentum of b and c. This set of momenta are called Jacobi-momenta^{3,5}. μ_a denotes the reduced mass of the system (a,bc). θ is the scattering angle, i.e., the angle between \vec{p}_3 and \vec{p}'_3 . Summation over m and m' has removed the dependence of the differential cross-section on the azimuthal angle. $T^{(s)}$ and $t^{(s)}$ are respectively the three body and two body transition matrix elements, s being the spectator atom. $\phi(\vec{q}_3)$ and $\phi'(\vec{q}_3)$ are the initial and final state molecular wavefunctions in the momentum representation.

We have shown⁸ how the integral in Eq.(2) can be evaluated without any approximations. We start by expanding the two body t-matrix element in a spherical harmonics expansion in the unit vector \hat{q}_3 ,

$$\langle \vec{q}'_s | t^{(s)} | \vec{q}_s \rangle = \sum_{LM} t^{(s)}_{LM}(q_3, \vec{p}_1, \vec{q}) Y_{LM}(\hat{q}_3), \quad (3)$$

with $t^{(s)}_{LM}$ given by

$$t^{(s)}_{LM}(q_3, \dots) = \int d\hat{q}_3 Y^*_{LM}(\hat{q}_3) \langle \vec{q}'_s | t^{(s)} | \vec{q}_s \rangle. \quad (4)$$

Substituting Eq.(3) in Eq.(2), after some algebra, we get

$$\begin{aligned} \langle \phi_3' | T^{(s)} | \phi_3 \rangle = & \sum_{\beta\lambda\gamma\mu LM} (qi)^\beta i^{(j-\lambda)} \left[\frac{j\hat{L}\hat{\beta}}{j'} \right]^{\frac{1}{2}} Y^*_{\beta\gamma}(\hat{q}) N^{(s)}_{LM\lambda\beta}(q) \\ & \times C(jL\lambda; 00) C(jL\lambda; mM\mu) C(\lambda\beta j'; 00) C(\lambda\beta j'; \mu\gamma m'), \end{aligned} \quad (5)$$

where q means + sign for $s=1$ and - sign for $s=2$, \vec{q} is the momentum transferred during the collision, $j_p(2j+1)$, etc., C 's are the Clebsch-Gordan coefficients⁹, and

$$N^{(s)}_{LM\lambda\beta}(q) = \int_0^\infty dr r^2 j_\beta(|\alpha_s|rq) K^{(s)}_{LM\lambda}(r) \chi_{v,j}(r). \quad (6)$$

with $\alpha_s p(-)^s \frac{m_s}{(m_1+m_2)}$, and

$$K^{(s)}_{LM\lambda}(r) = \frac{2}{\pi} \int_0^\infty dq_3 q_3^2 j_\lambda(q_3 r) t^{(s)}_{LM}(q_3) I_{v,j}(q_3), \quad (7)$$

$$I_{v,j}(q_3) = \int_0^\infty dr r^2 \chi_{v,j}(r) j^* j(q_3 r), \quad (8)$$

$\chi_{v,j}(r)$ being the radial part of the vibration-rotation wavefunction and j_j is the spherical Bessel function of order j .

To simplify the remaining algebra it is convenient to choose the z-axis of the coordinate system along \vec{q} , the direction of momentum transfer. Then

$$Y_{\beta\gamma}^*(\hat{q}) = \left(\frac{\hat{\beta}}{4\pi}\right)^{\frac{1}{2}} \delta_{\gamma 0}. \quad (9)$$

Using the properties of Clebsch-Gordan coefficients⁹, C's, and Racah coefficients, W's, Eq.(5) can be rewritten as

$$\begin{aligned} \langle \phi_3' | T^{(s)} | \phi_3 \rangle = & \sum_{\beta \lambda L J} (qi)^{\beta} i^{(J-\lambda)} \left[\frac{j \hat{L} \lambda \hat{J}}{4\pi j'} \right]^{\frac{1}{2}} \hat{\beta} N_{LM\lambda\beta}^{(s)}(q) C(jL\lambda; 00) \\ & \times C(\lambda\beta j'; 00) C(jJj'; mM) C(L\beta J; M0) W(jLj'\beta; \lambda J). \end{aligned} \quad (10)$$

The C and W coefficients express the relation between the total angular momentum change during the collision J and the initial and final rotational quantum numbers, j and j'. We also note the total angular momentum change J is composed of two parts, L coming from the two body t-matrix and β , the usual component, derived from the momentum transferred during the collision.

The expression for the differential cross-section is now obtained by summing the absolute square of the collision amplitude over m and $M=m'-m$ leading to,

$$\frac{d\sigma}{d\Omega}(vj\mathbf{p}_3 \rightarrow v'j'\mathbf{p}_3', \theta) = \left(\frac{2\pi}{\hbar}\right)^4 \mu_3^2 \frac{p_3'}{p_3} \sum_{J=|j-j'|}^{J=j+j'} \sum_M |F_{JM}|^2, \quad (11)$$

where,

$$F_{JM} = \sum_{L\beta\lambda} (i)^{(J-\lambda+\beta)} \hat{\beta} \left[\frac{\hat{L}\hat{\lambda}}{4\pi} \right]^{\frac{1}{2}} C(jL\lambda; 00) C(\lambda\beta j'; 00) C(L\beta J; M0) \\ \times W(jLj'\beta; \lambda J) [N_{LM\lambda\beta}^{(1)} + (-1)^{\beta} N_{LM\lambda\beta}^{(2)}] \quad (12)$$

In contrast, the differential cross-section in the peaking approximation is given by³

$$\left[\frac{d\sigma}{d\Omega} (vj p_3 \rightarrow v' j' p'_3, \theta) \right]_{PA} = \left(\frac{2\pi}{h} \right)^4 \mu_{\frac{p_3}{p_3}}^2 \sum_{\lambda=|j-j'|}^{\lambda=j+j'} \hat{\lambda} C^2(j\lambda j'; 00) \\ \times |f_{v'j',vj,\lambda}^{(1)} t_{PA}^{(1)} + (-1)^{\delta j} f_{v'j',vj,\lambda}^{(2)} t_{PA}^{(2)}|^2. \quad (13)$$

where

$$f_{v'j',vj,\lambda}^{(s)} p \int_0^{\infty} dr r^2 \chi_{v'j'}(r) j_{\lambda}(|\alpha_s| r q) \chi_{vj}(r). \quad (14)$$

The total cross-section is obtained from the differential cross-section by the relation

$$\sigma(vj p_3 \rightarrow v' j' p'_3) = \frac{2\pi}{p_3 p'_3} \int_{p_3 - p'_3}^{p_3 + p'_3} \left(\frac{d\sigma}{d\Omega} \right) q dq. \quad (15)$$

Eq.(11) is our result for an impulse calculation without further approximations, whereas eq.(13) is the standard PA result. To compare the two sets of calculations we pick a hard core potential to represent the two-body interaction. The two-body t-matrix for this potential is available in a closed

form¹⁰ and is, in fact, the only potential used in the previous atom-diatom studies. We compare the results for a system extensively studied previously^{3,6}



The computations have been performed for initial vibrational level $v=0$ and final levels $v'=0, 1$, and 2 . For relative kinetic energy of 1 eV , the hard core radius is taken to be³ 1.62 \AA . In PA, for homonuclear diatomic molecules, the product of the initial and final wavefunctions is assumed to peak at the mid-point of their two centers, $q_3=0$ and $q_3'=0$, and the two-body t-matrix is evaluated at fixed internal momentum $\vec{q}_3 = \frac{1}{4}\vec{q}$, where $\vec{q} = \vec{p}_3' - \vec{p}_3$ is the momentum transferred during the collision.

Molecular wavefunctions used in this calculation were obtained by numerical integration of the radial Schrödinger equation¹¹ using RKR diatom potential constructed from spectroscopic constants¹². Previous work used harmonic oscillator potential to obtain the diatom wavefunctions. There are substantial differences between peaking calculations using harmonic oscillator and more accurate wavefunctions for situations involving large vibrational-rotational inelasticity. To highlight the differences between the peaking and exact IA calculations we used more accurate wavefunctions throughout this work.

Fig.1 gives a plot of the differential cross-section for the process $(0,0 \rightarrow 1,6)$ as function of scattering angle θ . For forward scattering the exact IA result is about two orders of magnitude smaller than the PA result! Even though the peaks and valleys for the two calculations track each other closely the discrepancy between the two sets of calculations is visible even on the log scale. The quantitative difference between the two calculations is best described by the ratio ρ of the exact/PA results, displayed in fig. 2. It is clear from this figure, which also displays this ratio for $(00 \rightarrow 0j')$, $j'=0,10$, and 20, that, except for elastic $(00 \rightarrow 00)$ scattering, there are noticeable differences between the two calculations. These differences appear to increase with energy loss, independent of whether the energy ends up in vibration or rotation. Further, even for large angles PA overestimates the exact results by about 15%.

Fig. 3 displays the total cross-section $\sigma_T(00 \rightarrow n'j')$ for $n'=0,1$, and 2 as function of energy loss. PA grossly overestimates the true result for small j' for $n'=1$ and 2. This is because small Δj scattering is essentially forward scattering for which the two calculations give very different results. The total cross-section mirrors this disparity, weight factor $\sin \theta$ notwithstanding. For large j' , when almost all the energy loss goes into molecular rotation

EXACT vs. PEAKING

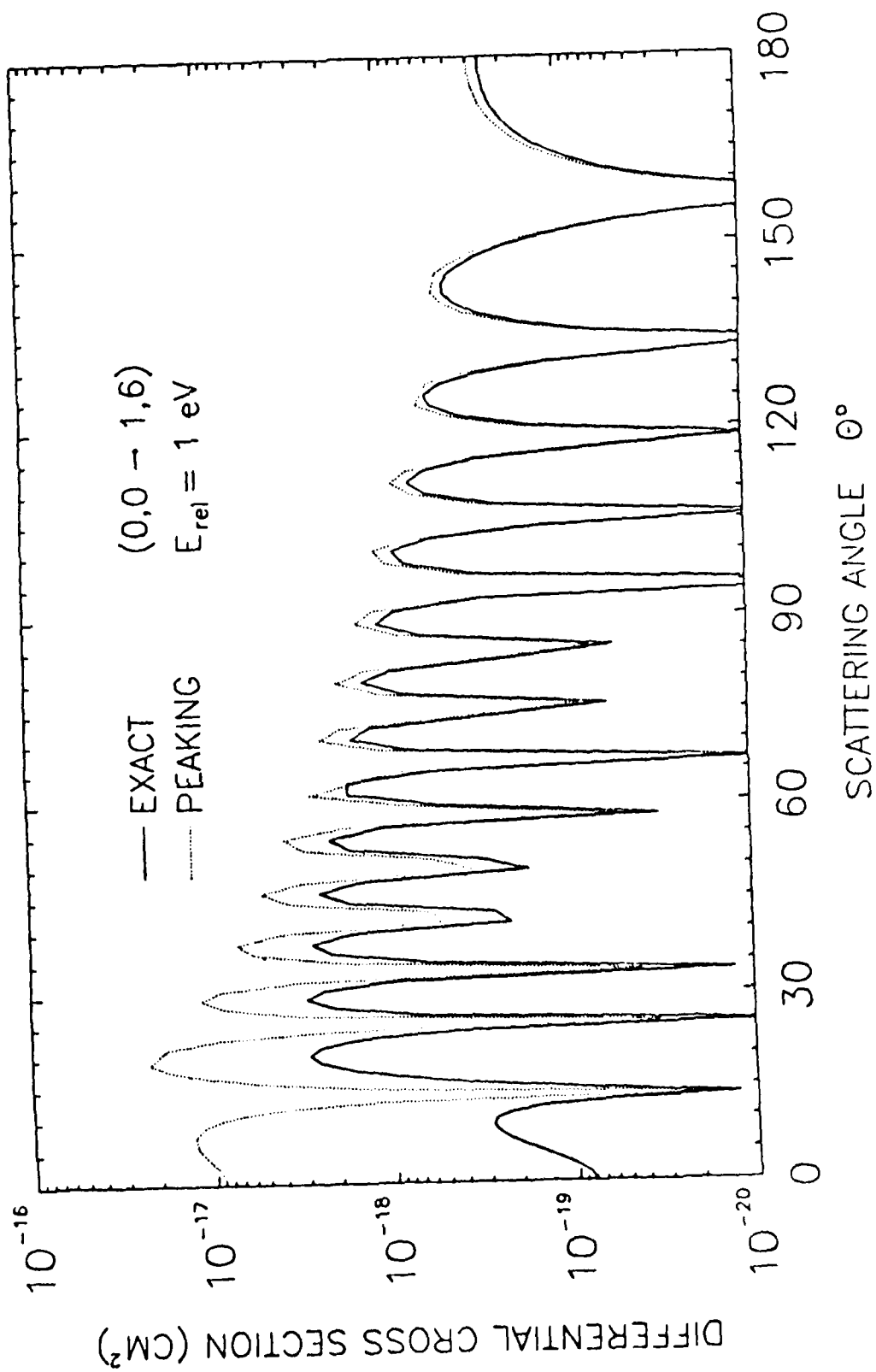


FIGURE A-1

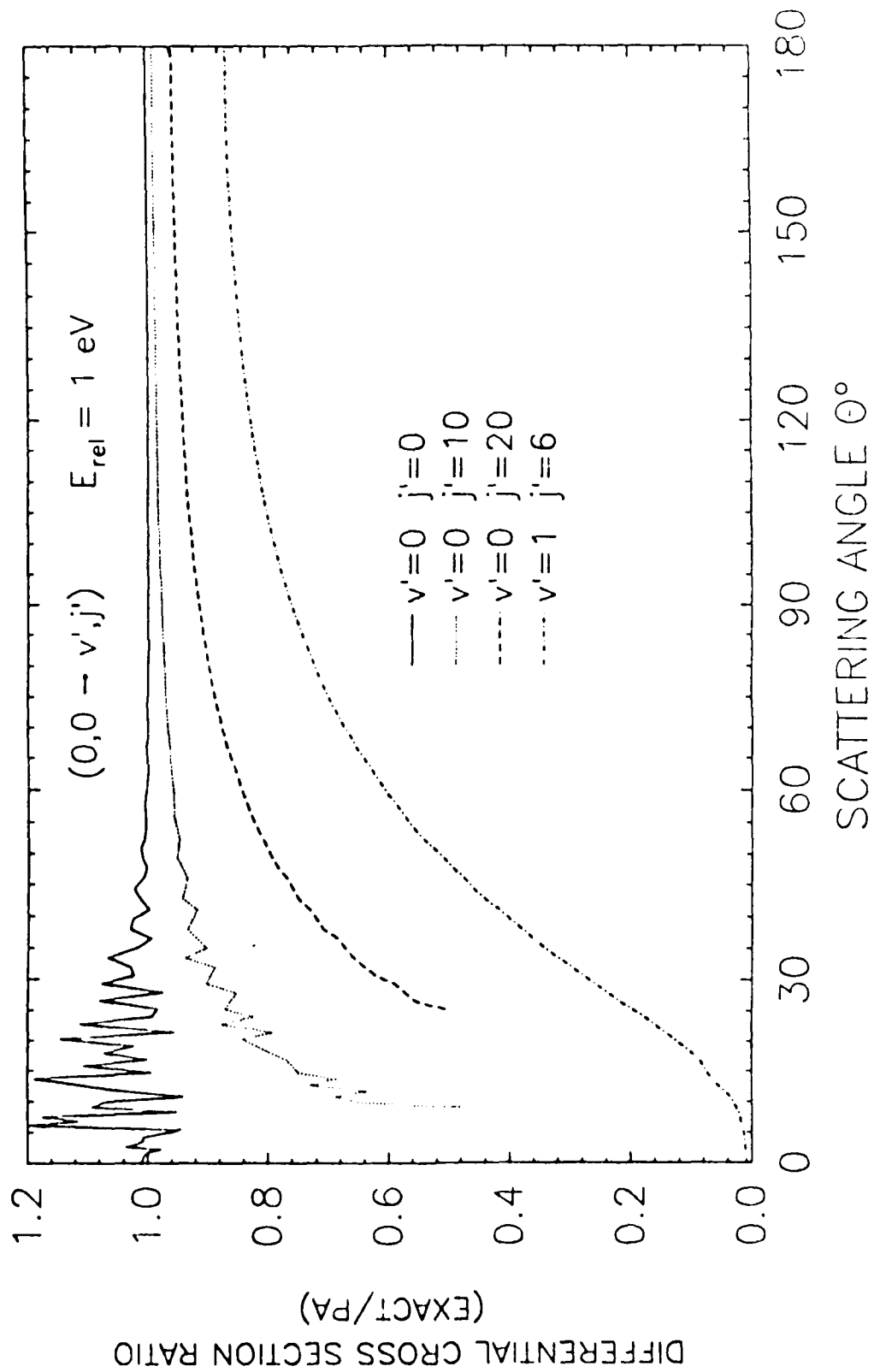


FIGURE A-2

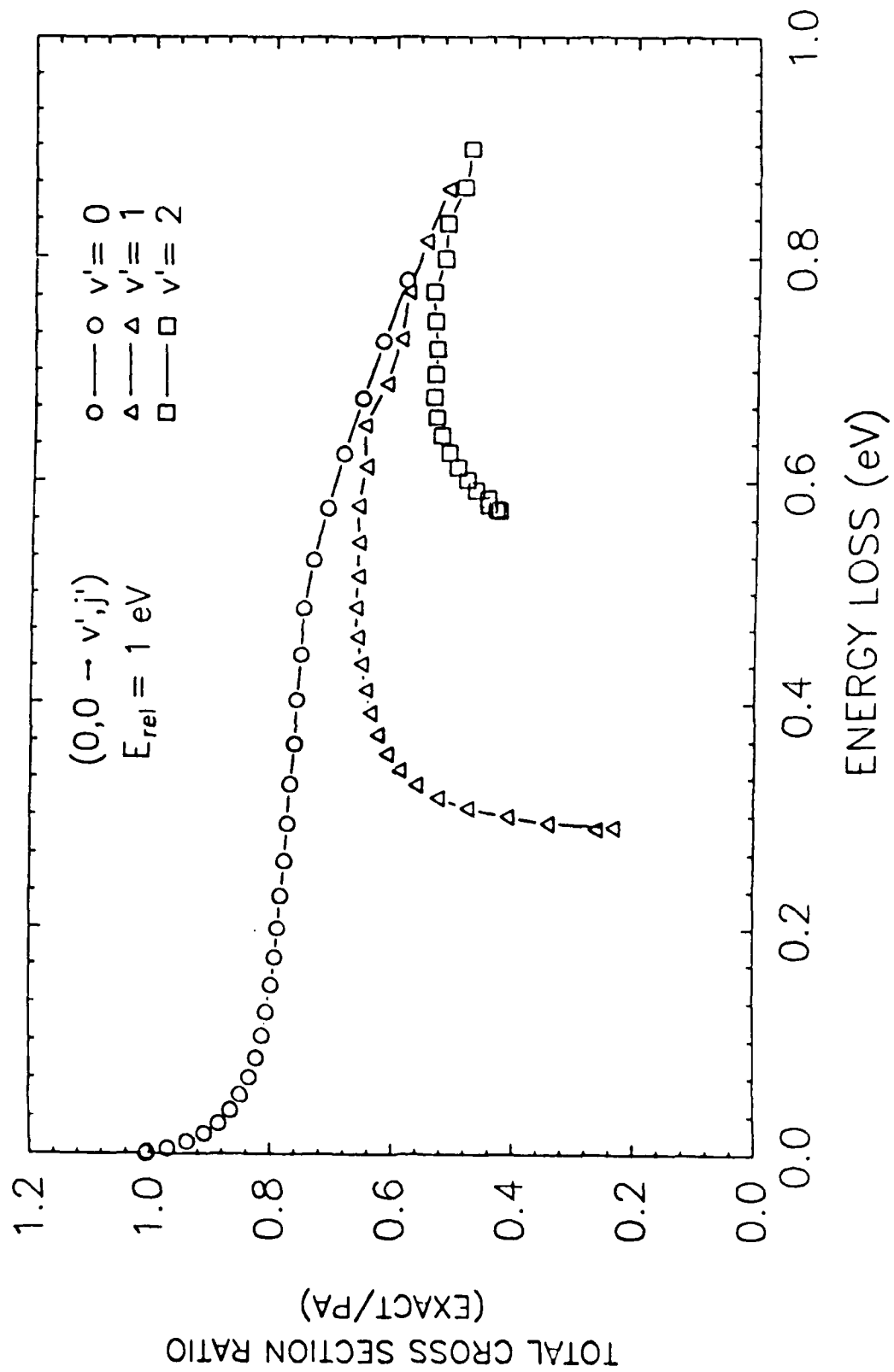


FIGURE A-3

APPENDIX B

CRITERIA FOR APPLICABILITY OF THE IMPULSE APPROACH TO COLLISIONS

Ramesh D. Sharma, Optical/Infrared Technology Division,

Geophysics Laboratory, Hanscom Air Force Base, MA 01731

Pradip M. Bakshi, Physics Department, Boston College, Chestnut

Hill, MA 02167, and

Joseph M. Sindoni, Yap Analytics Inc., 594 Marrett Road,

Lexington, MA 02173.

ABSTRACT

Using an exact formulation of impulse approach (IA) to atom-diatom collisions we assess its internal consistency. By comparing the cross-sections in the forward and reverse directions for the vibrational-rotational inelastic processes, using the half-on-the-shell (post and prior) models of the two-body t -matrix, we show that in both cases the IA leads to a violation of the semi-detailed balance (sdb) condition for small scattering angles. An off-shell model for the two-body t -matrix, which preserves sdb, is shown to have other serious shortcomings. The cross-sections are studied quantitatively as a function of the relative translational energy and the mass of the incident particle, and criteria discussed for the applicability of IA.

PACS numbers:03.80.+r, 34.50.-s.

Introduction: Since its inception the Impulse Approach (IA) to collisions has been used in diverse fields of Physics¹⁻⁵. The conditions of its validity are often heuristically described, but quantitative measures of its applicability are not available. IA as applied to atom-molecule collisions to date⁴⁻⁶ consists of three-steps: (1) The multiple collision expansion is truncated, retaining only the single collision terms. (2) The three-body T-matrix element is replaced by a two-body t-matrix element. The choice of the energy parameter of the two-body t-matrix distinguishes the various models (e.g. post⁴, prior⁴, full⁵). (3) A further approximation, the Peaking Approximation (PA), was invoked in the earlier studies^{4,5} to evaluate the transition amplitude.

We have recently shown^{6,7} how to evaluate the transition amplitude without any approximations, eliminating the errors due to the last step. This now allows us to take a critical look at the choice of the energy parameter in the two-body t-matrix. In this paper we show that the two half-on-the-shell models⁴, prior and post, violate the semi-detailed balance (sdb) condition for small scattering angles, indicating an internal inconsistency in those approaches. We also show that the (off-shell) full model⁵, which satisfies sdb, has other serious shortcomings. We further suggest alternate models which satisfy sdb (and do not have other formal

difficulties) to test the model dependence of the cross-sections. Finally, we discuss criteria for the applicability of IA. The detailed results given here are obtained using a two-body interaction with a hard core potential^{4,5,8}. The conclusions reached, however, should be applicable to other potentials as well.

In a multiple collision expansion⁴ of the atom-diatom three-body T-matrix,

$$T(z) = T^{(1)} + T^{(2)} + T^{(1)}G_3T^{(2)} + T^{(2)}G_3T^{(1)} + \dots, \quad (1)$$

where $G_3 = (z - H_3)^{-1}p(z - H_0 - V_3)^{-1}$ is the propagator corresponding to the atom-diatom Hamiltonian which includes the relative translational energy and a potential energy V_3 of the molecule 1-2 but not the interaction energy of the incident atom with atoms 1 (V_1) and 2 (V_2) of the diatom. The first two terms correspond to the collision of the incident atom 3 with atoms 2 and 1 respectively, while atoms 1 and 2 are the spectators, indicated by superscripts. The next two terms represent the double collision terms.

IA retains only the two single collision terms⁴⁻⁶. The second, and crucial, step in IA is the reduction of the three-body T-matrix to the two-body t-matrix by assuming that the time duration of the collision is much shorter than the characteristic times for the molecular motion. The function of the intramolecular potential is then to generate a momentum distribution for the two atoms constituting the diatom. Formally, the two steps are represented by^{4,5}

$$\langle \phi'_3 | T | \phi_3 \rangle \Rightarrow \langle \phi'_3 | T^{(1)} + T^{(2)} | \phi_3 \rangle, \quad (1)$$

and

$$\langle \phi'_3 | T^{(s)}(E) | \phi_3 \rangle \Rightarrow \int d\vec{q}_3 \phi'(\vec{q}'_3) \langle \vec{q}'_s | t^{(s)}(\epsilon_s) | \vec{q}_s \rangle \phi(\vec{q}_3), \quad (2)$$

where $|\phi_3\rangle \equiv |v, j, m, \vec{p}_3\rangle$ is the initial state, the final state being denoted by primes. E , the eigenvalue of H_3 , is the total energy of the initial (and final) state; $\epsilon_s = E_s = q_s^2 / (2m_u)$ is the relative kinetic energy of the non-spectator t and u atoms before the collision, \vec{p}_3 and \vec{p}'_3 are the momenta of the incident particle before and after the collision in the center-of-mass (CM) frame of the atom-molecule system. $T^{(s)}$ and $t^{(s)}$ respectively generate the three-body and two-body transition matrix elements, s being the spectator atom. $\phi(\vec{q}_3)$ and $\phi'(\vec{q}_3)$ are the initial and final state molecular wave-functions in the momentum representation. \vec{q}_s and \vec{q}'_s are the Jacobi momenta^{4,9} before and after the collision.

The choice $\epsilon_s = E_s$ (the kinetic energy of the colliding pair before collision) in the two-body t -matrix element

$$\langle \vec{q}'_s | t^{(s)}(\epsilon_s) | \vec{q}_s \rangle \equiv t^{(s)}(\vec{q}'_s, \vec{q}_s; \epsilon_s) \quad (3)$$

seems to be the natural one in the spirit of IA and is called the post form⁴ of IA. Other choices have been considered; $\epsilon_s =$

$E'_s = q'^2_s / (2m_{tu})$ is called the prior form⁴, m_{tu} being the reduced mass of the t and u atoms. The choice⁵ $\epsilon_s = E - p^2_s / 2\mu_s$, μ_s being the reduced mass of the s and (t+u) system, may be called the full form in that it subtracts the spectator atom energy from E, the total physical energy of the process. The post and prior forms are half-on-the-shell, since one of the momenta, \vec{q}_s or \vec{q}'_s ; lies on the energy shell. The full form is off-shell. The basic assumption of IA, that the spectator momentum p_s has not changed during the collision is incorporated in each case. Calculation of cross-sections using different ϵ_s will generally give different results. We return to this point later.

To compare the relative merits of different models, we apply symmetry considerations. Since the Hamiltonian is independent of time and quadratic in momenta, it is invariant under time reversal. Combined with the space inversion symmetry, this leads to the semi detailed balance (sdb) relation^{10,11} between the differential cross-sections for the forward and reverse processes,

$$p[d\sigma(i \rightarrow f)/d\Omega]/\rho(f) = p'[d\sigma(f \rightarrow i)/d\Omega]/\rho(i) \quad (4)$$

where $\rho(i)$ and $\rho(f)$ are the densities of state in the initial and final states; p and p' represent the incident flux densities. A valid theory must lead to cross-sections which satisfy Eq. (5).

Results: We have computed the differential cross-sections for the much studied process⁴⁻⁶



in the forward and reverse directions using IA, Eq. (3), with the previously employed^{4,5} hard core two-body (atom-atom) potential¹² for various values of the relative translational energies E_{rel} . In Figure 1 the differential cross-section using the post model, for the process $v=0 \ j=12 \rightarrow v=1 \ j=6$, in the forward direction at $E_{\text{rel}} = 1 \text{ ev}$ is given by the solid line. The cross-section for the reverse process multiplied by $p'_3 \rho(f) / p_3 \rho(i)$, the ratio of the densities of state times the incident flux ($\rho(f) \propto [(2j'+1)p_3']$ and $\rho(i) \propto [(2j+1)p_3]$), and termed 'normalized' reverse differential cross-section, is given by the dotted line. The two curves should be identical if the theory obeys sdb. Up to a scattering angle of about 50° the two curves do not appear related. From 50° to 70° the two curves have a similar structure. For larger scattering angles they are indistinguishable.

The dotted line in figure 2 gives a plot of the ratio of the two differential cross-sections of Figure 1 as a function of the scattering angle for E_{rel} of 1 ev, its departure from unity providing a quantitative measure of the violation of sdb. The solid line represents a similar ratio for $E_{\text{rel}} = 4 \text{ ev}$. It is clearly seen that the two curves which appear unrelated in Figure 1 show a definite periodicity in their ratio, and the whole structure gets squeezed towards smaller angles at higher

relative translational energy.

We conclude that the post form does not satisfy the sdb condition for small angles. If we use the prior form for ϵ_s , the forward process is represented by the dotted line in Fig. 1 and the normalized reverse process is represented by the solid line. Thus the prior form also fails to satisfy sdb where the post form fails. It can be shown from the structure of the post and prior t-matrix elements that the post \leftrightarrow prior interchange is equivalent to the forward \leftrightarrow (normalized) reverse interchange. The full form obeys sdb, a result predictable from the structure of its t-matrix.

Now we examine the mass dependence of the sdb violation. Figure 3 shows the ratio of the forward and normalized reverse differential cross-sections for the same N_2 transition caused by a collision with H atom (solid curve) or Li⁺ (dotted curve), both at E_{rel} of 1 ev, as functions of $r_c q$, $q = |\vec{p}_3' - \vec{p}_3|$ being the momentum transfer. This is a more convenient parameter to compare processes with different projectile masses. For $r_c q \geq 20$ the two curves show a period of π with the H atom curve having a smaller amplitude. The effect of a lighter incident particle appears similar to that of increasing the energy of relative motion as seen in Figure 2. Figure 4 displays $(r_c q)_1$, the smallest value of $r_c q$ at which sdb is satisfied to 1 % as function of relative energy¹² for the two incident particles

studied.

Discussion: We have shown above that both the post and prior forms violate the sdb criterion for small angles. The other model used in the literature⁵, the full form, does not violate sdb but poses other problems. The first is a conceptual difficulty; the choice $\epsilon_s = E - p_s^2/2\mu_s$ always leads to a negative energy ϵ_s for a part of the range of integration over \vec{q}_s in Eq.(3). Thus the amplitude integral in Eq.(3) remains ill-defined without introducing a cut-off (in the range of integration) or attempting analytical continuation into negative energies. Secondly, even if a cut-off is introduced as a practical measure, the full form leads to very high cross-sections for the smaller angles, yielding an unreasonably large total cross-section in significant excess of the quantum-mechanical shadow. The total cross-sections based on the post and prior forms, on the other hand, understate the shadow limit.

In view of these intrinsic difficulties with the models used in the literature, one can consider other ad hoc choices for ϵ_s which avoid some of these problems. An obvious choice is $\epsilon_s = \frac{1}{2}(E_s + E'_s)$, which may be termed the mean model. This introduces a symmetry in the structure of the t-matrix and the sdb criterion is automatically satisfied. It is also free from any definition problems. Figure 5 provides a comparison of these four models for the same process as in Figure 1 and 2 with

$E_{rel} = 4$ eV. The full model is evaluated by cutting off the range of \vec{q}_j where ϵ_s would become negative. For this energy, the wave functions' product in Eq.(3) in the excluded domain is quite insignificant, making this a practical calculation. (For an energy such as $E_{rel} = 1$ eV, the cut-off for the full model would take away a significant part of the form factor integral, making it a meaningless calculation.) It is clear from Figure 5 that for larger angles these results are model independent. For intermediate angles, the post, prior, and mean models trace similar patterns. For small angles the models vary significantly.

In conclusion, we suggest (1) the sdb condition and (2) model independence as two criteria to be employed in assessing the applicability of IA. In the domain I where both the criteria are met, one may use IA with confidence. Figure 4 provides the boundary of this domain for 1% accuracy for both the post and prior models. In the domain II, where the post, prior, and the mean models retain the same patterns with slight quantitative differences, IA may be expected to be a good approximation with any of these models, with possible errors of the same magnitude as their differences. The full model seems to overstate the cross-sections and seems much less reliable in this domain. For the small angles, domain III, all the models give rather different results. This is also the domain where

FIGURE CAPTIONS

FIG.1. Direct (solid line) and normalized reverse (dotted line) differential cross-sections for $\text{Li}^+ + \text{N}_2(v=0, j=12) \rightarrow \text{Li}^+ + \text{N}_2(v'=1, j'=6)$ at relative translational energy $E_{\text{rel}} = 1$ eV as a function of scattering angle θ° .

FIG.2. Ratio of the forward and normalized reverse differential cross-sections of Fig. (1) as function of scattering angle θ° at $E_{\text{rel}} = 1$ eV (dotted line) and $E_{\text{rel}} = 4$ eV (solid line).

FIG.3. Ratios of the forward and normalized Reverse differential cross-sections for the $(0,12) \rightleftharpoons (1,6)$ transitions of N_2 at relative translational energy of 1 eV for collision with Li^+ (dotted line) and H (solid line).

FIG.4. Threshold value of $r_c q$ for 1% deviation from semi-detailed balance condition as function of relative translational energy in eV for the $(0,12) \rightleftharpoons (1,6)$ transitions of N_2 . Dotted line is for collision with Li^+ and solid line is for collision with H.

FIG.5. Comparison of the differential cross-sections for the process $\text{Li}^+ + \text{N}_2(v=0, j=12) \rightarrow \text{Li}^+ + \text{N}_2(v'=1, j'=6)$ at relative translational energy of 4 eV for four models of ϵ_s : post(solid line), prior(dashed line), mean(dash-dot-dash) and full(tiny dashes).

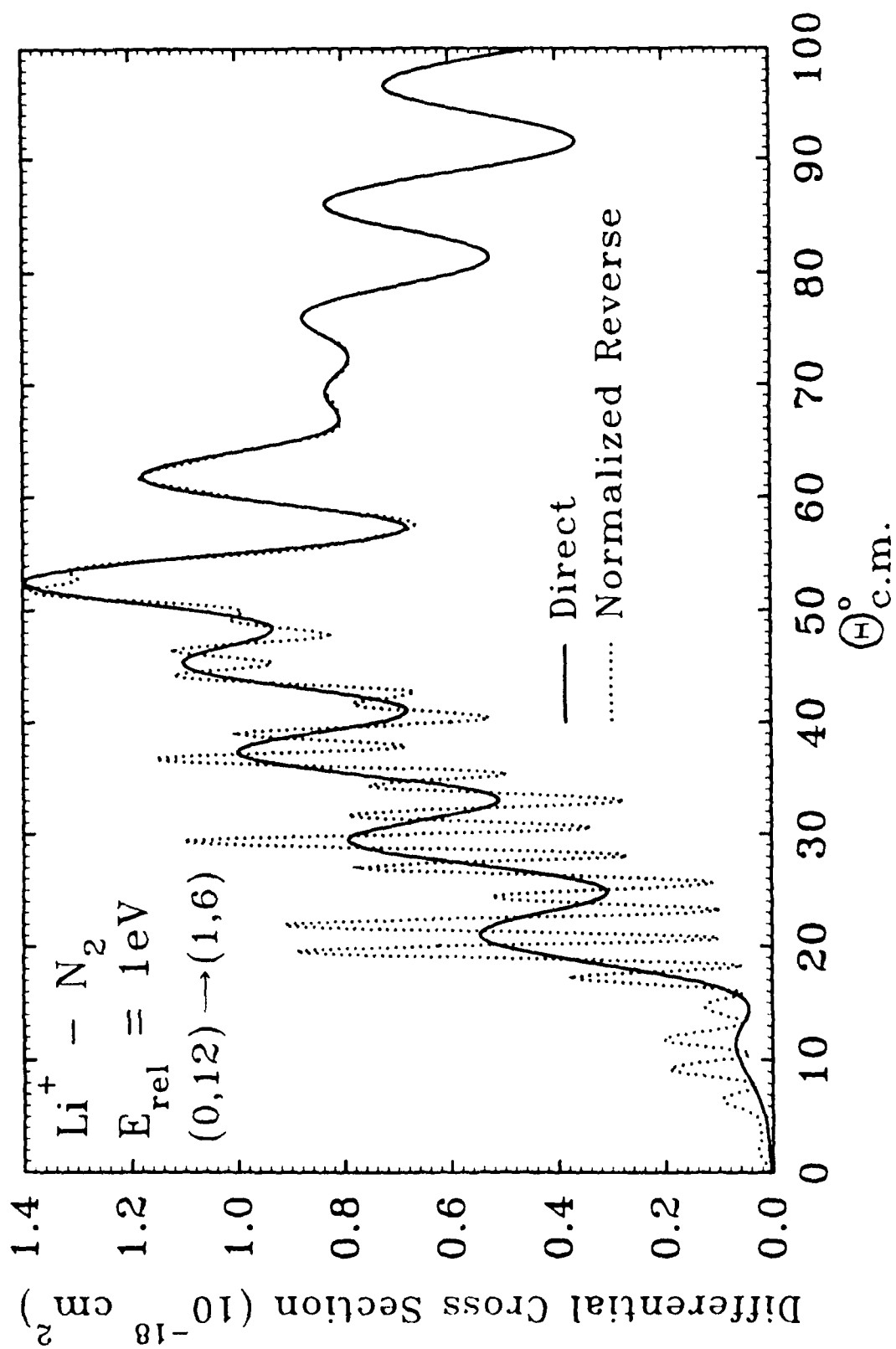


FIGURE B-1

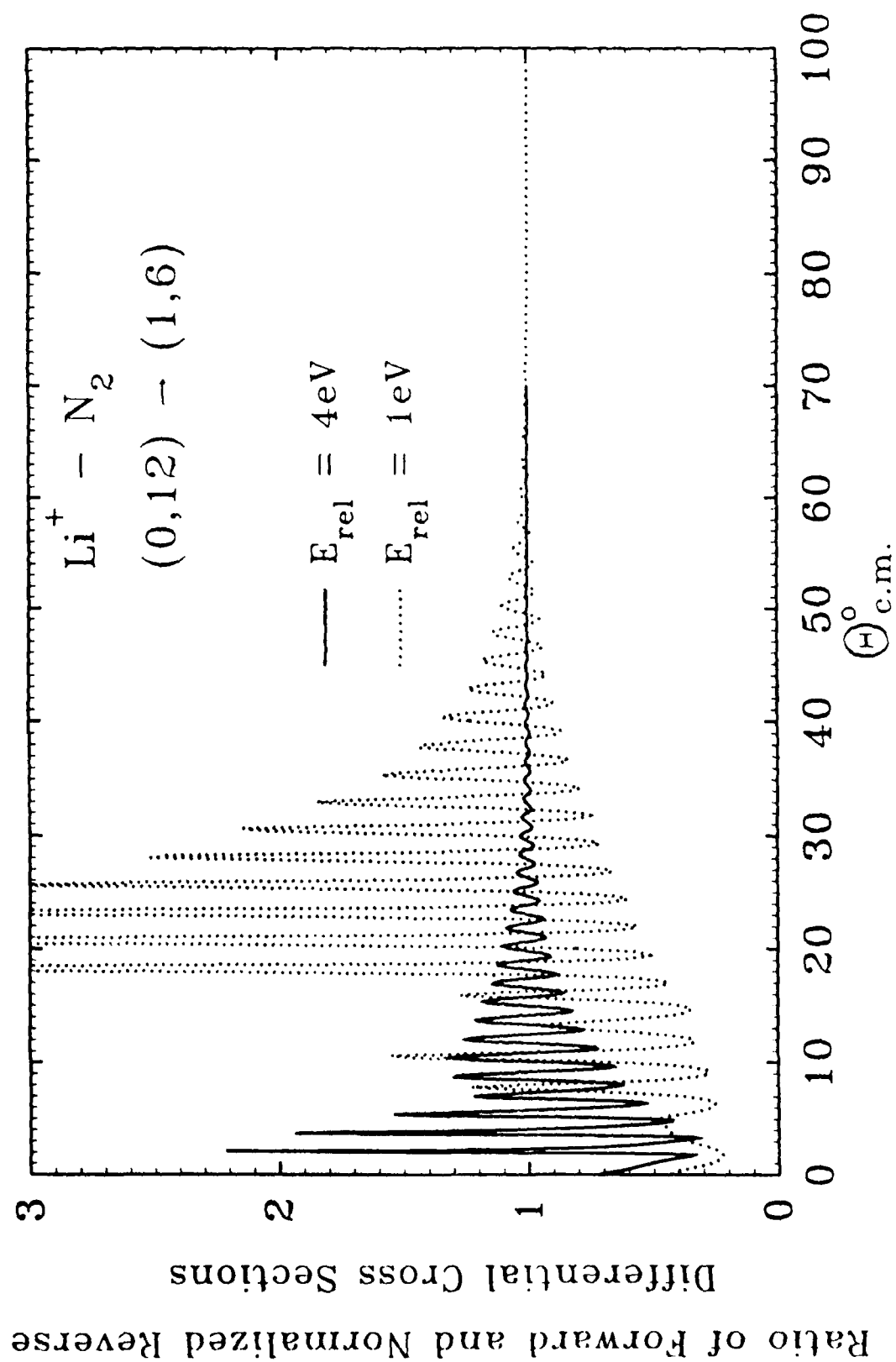


FIGURE B-2

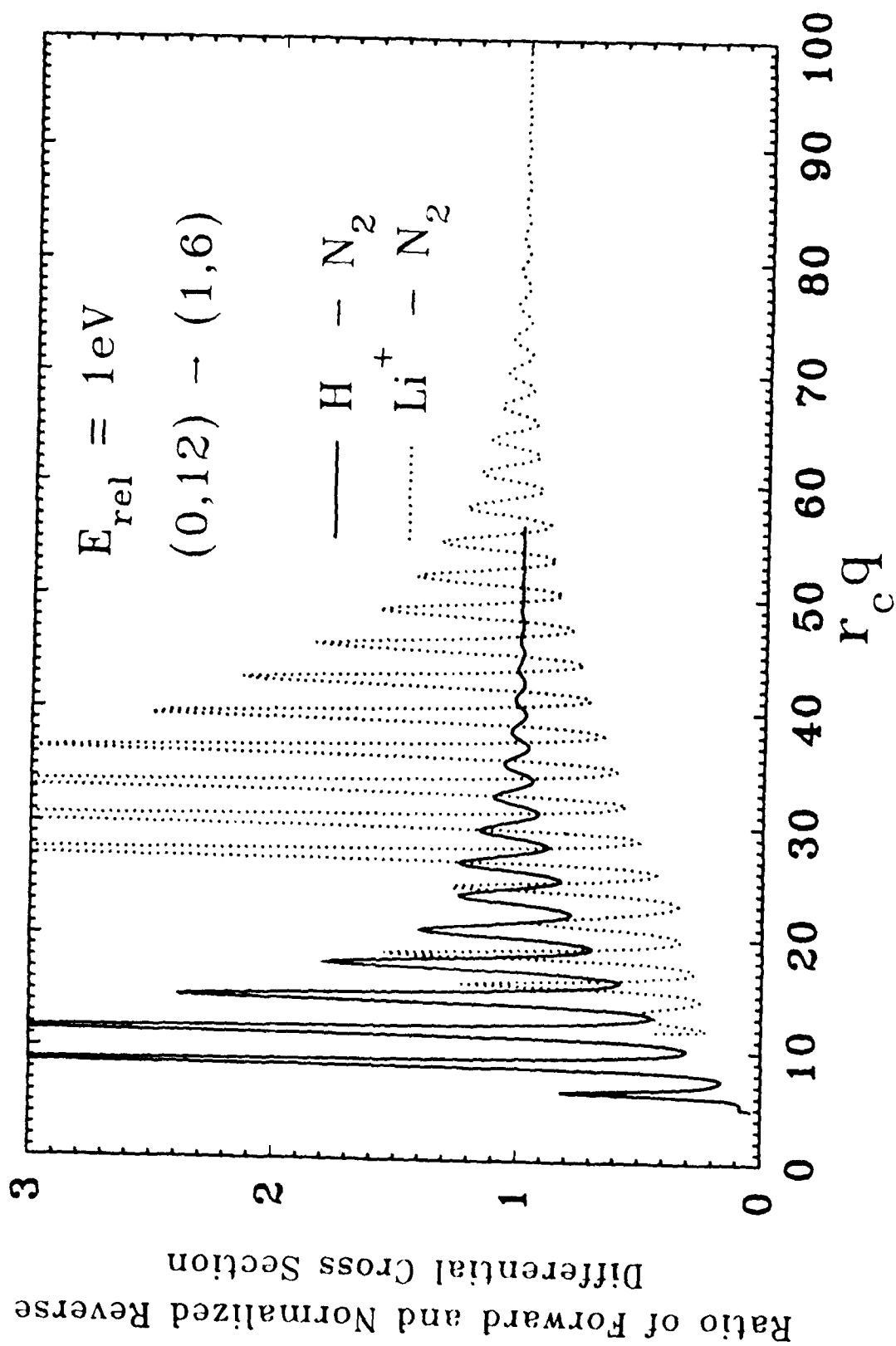


FIGURE B-3

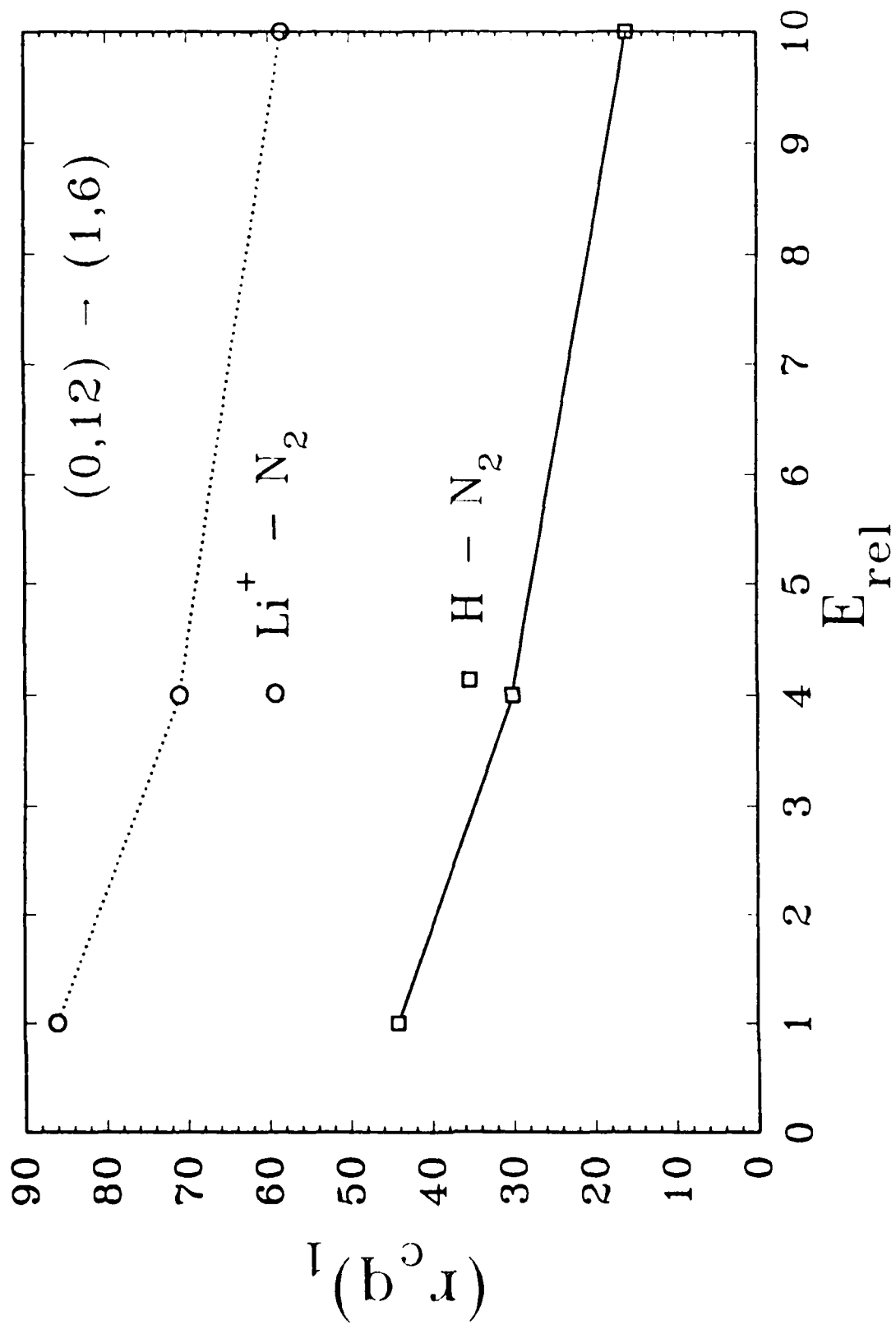


FIGURE B-4

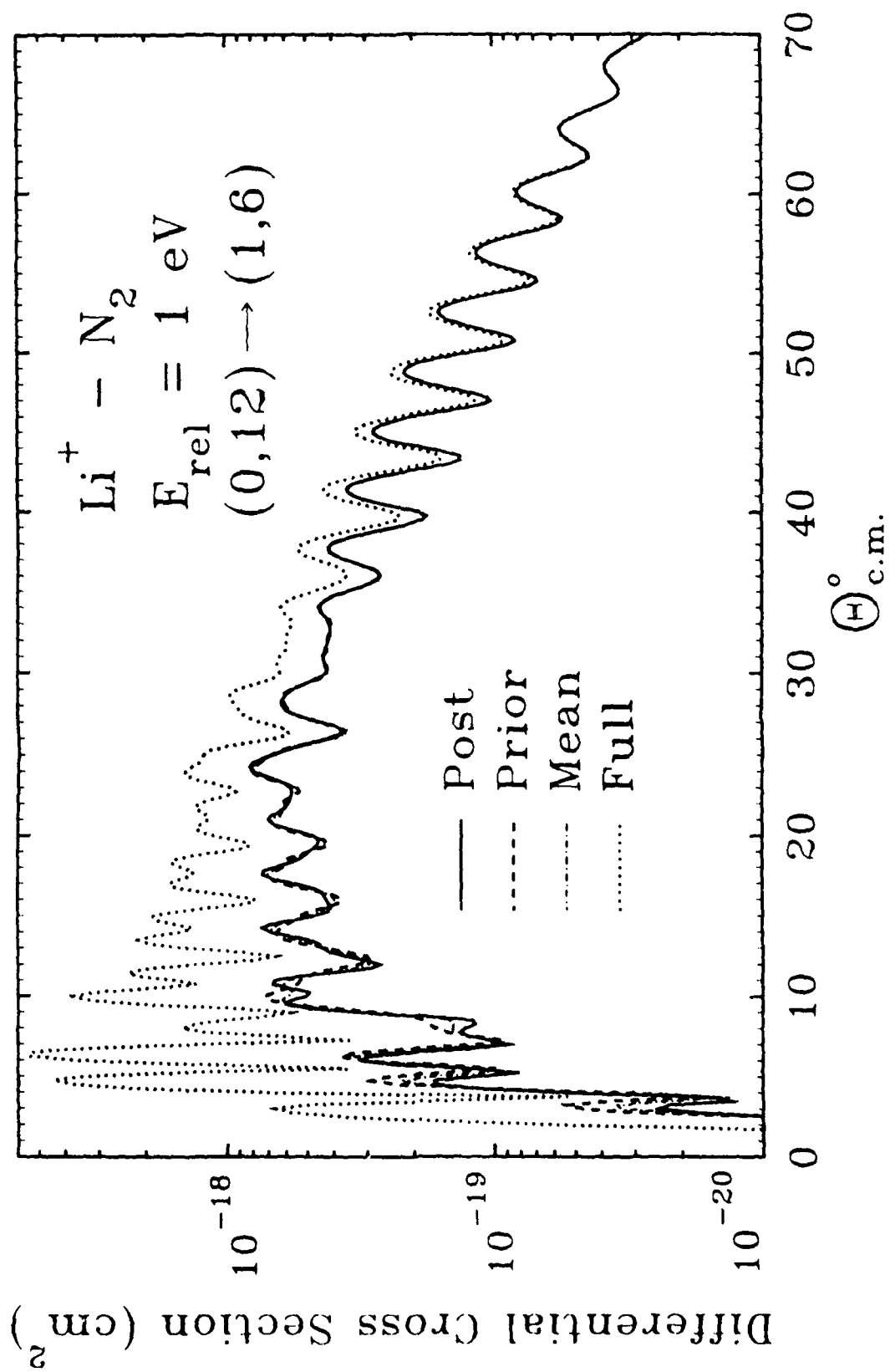


FIGURE B-5